

Giant Negative Thermal Expansion in Antiferromagnetic CrAs-Based Compounds

Yong Hu,^{1,2} Xinqi Zheng,³ Guodong Ma,^{1,2} Huiqing Lu,⁴ Lei Zhang,⁵ Changsheng Zhang,⁶ Yuanhua Xia,⁶ Yiqing Hao,⁷ Lunhua He,^{8,9} Jie Chen,¹⁰ Feiran Shen,⁸ Shouguo Wang,³ Cong Wang,⁴ Dunhui Wang,^{1,2,*} and Youwei Du^{1,2}

¹*National Laboratory of Solid State Microstructures and Jiangsu Key Laboratory for Nano Technology, Department of Physics, Nanjing University, Nanjing 210093, China*

²*Collaborative Innovation Center of Advanced Microstructures, Nanjing University, Nanjing 210093, China*

³*School of Materials Science and Engineering, University of Science and Technology Beijing, Beijing 100083, China*

⁴*Department of Physics, Center for Condensed Matter and Materials Physics, Beihang University, Beijing 100083, China*

⁵*Anhui Key Laboratory of Condensed Matter Physics at Extreme Conditions, High Magnetic Field Laboratory, Chinese Academy of Sciences, Hefei 230031, China*

⁶*Key Laboratory for Neutron Physics of Chinese Academy of Engineering Physics, Institute of Nuclear Physics and Chemistry, Mianyang 621999, China*

⁷*State Key Laboratory of Surface Physics and Department of Physics, Fudan University, Shanghai 200433, China*

⁸*Beijing National Laboratory for Condensed Matter Physics, Institute of Physics, Chinese Academy of Sciences, Beijing 100190, China*

⁹*Songshan Lake Materials Laboratory, Dongguan 523808, China*

¹⁰*China Spallation Neutron Source, Dongguan 523808, China*

(Received 2 August 2019; published 13 September 2019)

CrAs is a well-known superconductor, which shows a pronounced volume contraction around a Néel temperature (T_N) of 260 K. However, it has not been considered as a negative thermal expansion (NTE) material for industrial applications partially because the temperature window of its phase transition is limited and does not cover room temperature. We prepare some CrAs-based compounds ($\text{Cr}_{0.98}\text{Ni}_{0.02}\text{As}$, CrAs, and $\text{CrAs}_{0.91}\text{S}_{0.09}$) and investigate their linear NTE properties. By chemical modification, a giant NTE can be realized in this system with a broad temperature window of 218 K from 122 to 340 K. Typically, a linear NTE coefficient of $-28.3 \times 10^{-6}\text{K}^{-1}$ in a broad NTE operation-temperature window of 98 K (from 242 to 340 K) is obtained in the $\text{CrAs}_{0.91}\text{S}_{0.09}$ compound. In the region between 275 and 315 K around room temperature, the linear NTE coefficient ($-51.2 \times 10^{-6}\text{K}^{-1}$) remains nearly independent of temperature. In addition, the CrAs-based compounds show large thermal and electrical conductivities and their dimensions are insensitive to the external magnetic field. The aforementioned excellent properties suggest that the CrAs-based compounds can serve as an alternative type of NTE materials and have promising applications, especially in the magnetic field environment.

DOI: 10.1103/PhysRevApplied.12.034027

I. INTRODUCTION

Negative thermal expansion (NTE) is a thermodynamic phenomenon in which some materials contract upon heating rather than expand as most materials do. NTE materials have attracted more and more attention due to their wide applications in printed circuit boards, machinery parts, optical fiber reflective grating devices, and high-precision optical mirrors [1,2]. In general, the materials with good NTE performance should first have a large linear NTE

coefficient (α). In addition, in order to avoid the thermal stress, NTE materials with high thermal conductivity are more desirable since they can conduct heat quickly and keep the temperature uniform [3,4]. With the increasing development of NTE materials, sometimes they should work in magnetic, electrical, or photic environments. Thus for the requirement of precision, their dimensions should be insensitive to these external stimuli [4]. Recently, a giant NTE has been detected in many types of functional materials, including the well-known ZrW_2O_8 family [1], CuO nanoparticles [5], PbTiO_3 -based compounds [6], $(\text{Bi}, \text{La})\text{NiO}_3$ [7], reduced layered ruthenate [8],

*wangdh@nju.edu.cn

and transition-metal cyanide framework systems (i.e., $\text{Ag}_3[\text{Co}(\text{CN})_6]$) [9]. However, only a few of these materials have been used in practice due to their low thermal conductivity. In order to overcome this problem, we begin to explore metals with large NTEs. Among them, the typical systems are magnetic phase transition metals, such as $\text{La}(\text{Fe}, \text{Si})_{13}$ -based and $\text{MnCo}_{0.98}\text{Cr}_{0.02}\text{Ge}$ alloys [3,10], in which a large NTE performance stems from the magneto-volume effect. Unfortunately, their dimensions are highly sensitive to an external magnetic field due to the obvious magnetostriction [11] or magnetostrain [12] effects, which is a negative factor to the precision instrument in a magnetic environment [4]. In this sense, developing antiferromagnetic (AFM) metal materials with good NTE properties is greatly desirable [4,13,14].

CrAs is one of the intermetallic pnictides with a MnP-type structure at ambient conditions, whose crystallographic and magnetic properties have been extensively investigated since the 1960s. This compound undergoes an AFM transition around the Néel temperature (T_N) of about 260 K and has a double-helical magnetic structure propagating along the orthorhombic c axis below T_N [15–17]. Very recently, pressure-induced superconductivity was observed in this compound, which generates great interest in understanding microscopic magnetic properties and their interplay with superconductivity [18–20]. In addition, we notice that an abrupt and giant volume contraction ($\Delta V/V \sim -2.4\%$) occurs in CrAs around T_N due to the coupled structural, magnetic, and electronic degrees of freedom [21,22], which makes it a promising candidate as a NTE material. However, the magnetovolume effect in CrAs appears only around 260 K. Thus, the working temperature window of this compound is limited and does not cover room temperature, which hinders its industrial applications to a large extent. It is reported that by doping a small amount of Ni or S in a CrAs compound, T_N would shift to lower or a higher temperature, respectively [21,22]. In this paper, we prepare a series of CrAs -based compounds, $\text{Cr}_{0.98}\text{Ni}_{0.02}\text{As}$, CrAs , and $\text{CrAs}_{0.91}\text{S}_{0.09}$, and investigate their NTE properties. The experimental results demonstrate that the NTE operation-temperature window of this system is successfully extended to 218 K (between 122 and 340 K) by chemical modification. Moreover, a large α of $-28.3 \times 10^{-6} \text{ K}^{-1}$ is achieved in the $\text{CrAs}_{0.91}\text{S}_{0.09}$ compound in the temperature range from 242 to 340 K, which includes room temperature. Strikingly, in the temperature region between 275 and 315 K, its value of α ($-51.2 \times 10^{-6} \text{ K}^{-1}$) remains nearly independent of temperature.

II. EXPERIMENT

Polycrystalline samples are prepared in the following ways: powders of Cr (99.9%, Aladdin), Ni (99.9%, Aladdin), As (99.99%, Aladdin), and S (99.9%, Aladdin)

are mixed in the desired proportions and sealed in evacuated silica tubes. Then the samples are heated at 1173 K for 3 days. After that, the reacted products are crushed and tableted under a pressure of 10 MPa to form a cylinder. The cylinder samples are then homogenized by annealing in evacuated quartz tubes under argon at 1173 K for 3 days and slowly cooled to room temperature at a rate of 1 K min^{-1} . The structure and lattice parameters are characterized by x-ray diffractometer (XRD) (TTR3, Rigaku, Japan) with $\text{Cu K}\alpha$ radiation at different temperatures. All XRD patterns are refined by the Rietveld method using the general structure analysis system (GSAS) suite of programs [23]. Linear thermal expansion data ($\Delta L/L$) versus temperature curves are obtained by a thermodilatometer (NETZSCH, DIL 402PC, Bavaria, Germany) with a heating rate of 2 K/min. The electrical resistivity and thermal conductivity are measured using a physical properties measurement system (Model 6000, Quantum Design, United States). The temperature dependence of magnetic susceptibility ($\chi-T$) is measured by a superconducting quantum interference device (SQUID, Quantum Design, United States). Differential scanning calorimetry (DSC) curves for the samples are measured by a DSC 204 F1(Netzsch, Germany) with a heating rate of 10 K min^{-1} . The neutron diffraction measurements for the CrAs sample are performed on a High Resolution Neutron Diffractometer (HRND) at China Mianyang Research Reactor (CMRR) [24]. The data are collected in the 2θ range of 20° – 160° at a neutron wavelength of 1.884 \AA . All neutron diffraction patterns are refined by using the FULLPROF suite to identify the crystal and the magnetic structures. Neutron powder diffraction experiments for $\text{Cr}_{0.98}\text{Ni}_{0.02}\text{As}$ and $\text{CrAs}_{0.91}\text{S}_{0.09}$ are performed on the time-of-flight diffractometer GPPD (the general purpose powder diffractometer) at CSNS (the China Spallation Neutron Source), Dongguan, China. Samples are loaded in 9.1-mm vanadium cans and patterns are collected with wavelength bands of 0.1 – 4.9 \AA .

III. RESULTS AND DISCUSSION

$\chi-T$ curves for the samples are measured in a magnetic field of 1000 Oe. It is well known that, in CrAs -based compounds, T_N cannot be determined by $\chi-T$ curves because no remarkable anomaly can be found around the AFM phase transition [25,26]. As shown in the Supplemental Material [27], the magnetic susceptibility increases with increasing temperature and no obvious peaks are observed in $\chi-T$ curves, which can be ascribed to the itinerant electron magnetism of these compounds [25,26]. Actually, the AFM transition temperatures of CrAs -based compounds are usually determined by thermal, electric, or structural measurements [25,28]. The Supplemental Material [27] shows the DSC curves for the samples. The values of T_N are estimated to be 188, 254, and 297 K on heating

for $\text{Cr}_{0.98}\text{Ni}_{0.02}\text{As}$, CrAs, and $\text{CrAs}_{0.91}\text{S}_{0.09}$, respectively, which are consistent with the earlier reports [21,22].

Figures 1(a)–1(c) display $\Delta L/L$ (reference temperature: 122 K) as a function of temperature for $\text{Cr}_{0.98}\text{Ni}_{0.02}\text{As}$, CrAs, and $\text{CrAs}_{0.91}\text{S}_{0.09}$, respectively. It can be seen that for each sample, there exists a temperature region in which the value of $\Delta L/L$ increases with decreasing temperature, suggesting the occurrence of NTE. For the CrAs sample, it exhibits a giant NTE in a temperature range from 197 to 283 K and the NTE operation-temperature window is 86 K. The maximum absolute value of $\Delta L/L$ is estimated to be 5.3×10^{-3} , which is larger than that of antiperovskite manganese nitride Mn_3GaN (3.8×10^{-3}) [29] and NaZn_{13} -type $\text{LaFe}_{11.5}\text{Si}_{1.5}$ (3.5×10^{-3}) [3]. As a result, the average value of α reaches up to $-61.9 \times 10^{-6} \text{ K}^{-1}$, which is shown in Fig. 1(b). In the case of $\text{Cr}_{0.98}\text{Ni}_{0.02}\text{As}$, T_N is remarkably decreased to 188 K by the substitution of Ni for Cr. As shown in Fig. 1(a), the maximum absolute value of $\Delta L/L$ amounts to 4.5×10^{-3} with an operation-temperature window of 105 K from 122 to 227 K, which corresponds to an average value of α of $-43.0 \times 10^{-6} \text{ K}^{-1}$ for $\text{Cr}_{0.98}\text{Ni}_{0.02}\text{As}$. In order to extend the working temperature region to cover room temperature, As atoms are partially replaced by S atoms, which

results in an increased T_N of 297 K in $\text{CrAs}_{0.91}\text{S}_{0.09}$. As shown in Fig. 1(c), the NTE operation-temperature window of $\text{CrAs}_{0.91}\text{S}_{0.09}$ is located between 242 and 340 K, which demonstrates a broad temperature range of 98 K including room temperature. It is found that the NTE operation-temperature windows of $\text{Cr}_{0.98}\text{Ni}_{0.02}\text{As}$ (105 K) and $\text{CrAs}_{0.91}\text{S}_{0.09}$ (98 K) are obviously broader than that of CrAs (86 K), which can be attributed to the induced defects and disorders of the component by the substitutions [8]. The maximum absolute value of $\Delta L/L$ for $\text{CrAs}_{0.91}\text{S}_{0.09}$ is 2.8×10^{-3} and the average value of α reaches up to $-28.3 \times 10^{-6} \text{ K}^{-1}$, which is about three times larger than that of the commercial NTE materials currently used, that is, ZrW_2O_8 with $\alpha = -8.8 \times 10^{-6} \text{ K}^{-1}$ [1]. It is worth noting that at room temperature, the absolute magnitude of this α is comparable to the high expansion metal of Al ($23 \times 10^{-6} \text{ K}^{-1}$ at room temperature), which is very meaningful for the design of precisely tailored thermal expansion or even zero expansion materials. More importantly, in the region between 275 and 315 K around room temperature, the value of α ($-51.2 \times 10^{-6} \text{ K}^{-1}$) remains almost independent of temperature, which is appreciable for practical applications [10]. From Figs. 1(a)–1(c), we find that the NTE operation-temperature windows of all the samples are just adjacent, demonstrating that a very broad working temperature region of 218 K from 122 to 340 K can be achieved in CrAs-based compounds by chemical modification.

Temperature-dependent XRD measurement is a more precise method to characterize NTE since it can detect the variation of lattice constant without the influence of cracks and density in the samples. As shown in the Supplemental Material [27], all the samples crystallize in the orthorhombic MnP-type structure in the measuring temperature range from 100 to 350 K. The structural parameters such as the lattice constants (a , b , and c) and the unit-cell volume (V) are achieved from the refined results based on XRD measurements. As shown in the Supplemental Material [27], some discontinuous changes of structural parameters are observed, which suggests the occurrence of an AFM phase transition in the temperature ranges of (150–200 K), (240–270 K), and (270–320 K), for $\text{Cr}_{0.98}\text{Ni}_{0.02}\text{As}$, CrAs, and $\text{CrAs}_{0.91}\text{S}_{0.09}$, respectively [28]. It is clearly shown that in the phase transition temperature region, the a axis and c axis show an abrupt jump while the b axis exhibits a sharp drop with increasing temperature. Compared to the changes of the a axis and c axis, the variation of the b axis around the phase transition temperature is much larger. For example, in the case of CrAs at T_N , the lattice constant changes are 0.3%, −3.5%, and 0.9% for the a axis, b axis, and c axis, respectively. As a result, V contracts with the increase in temperature and indicates a NTE behavior, which is ascribed to the decrease in the b axis. For comparing with the directly measured NTE results by dilatometer, we calculate the values of $\Delta V/V$. As shown in Fig. 2, the

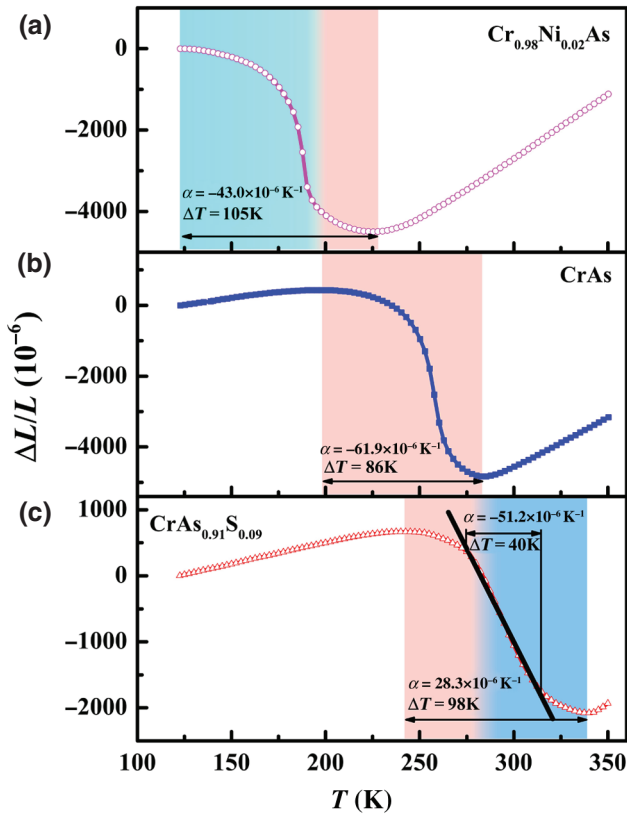


FIG. 1. Temperature dependence of linear thermal expansions $\Delta L/L$ (reference temperature: 122 K) for (a) $\text{Cr}_{0.98}\text{Ni}_{0.02}\text{As}$, (b) CrAs, and (c) $\text{CrAs}_{0.91}\text{S}_{0.09}$.

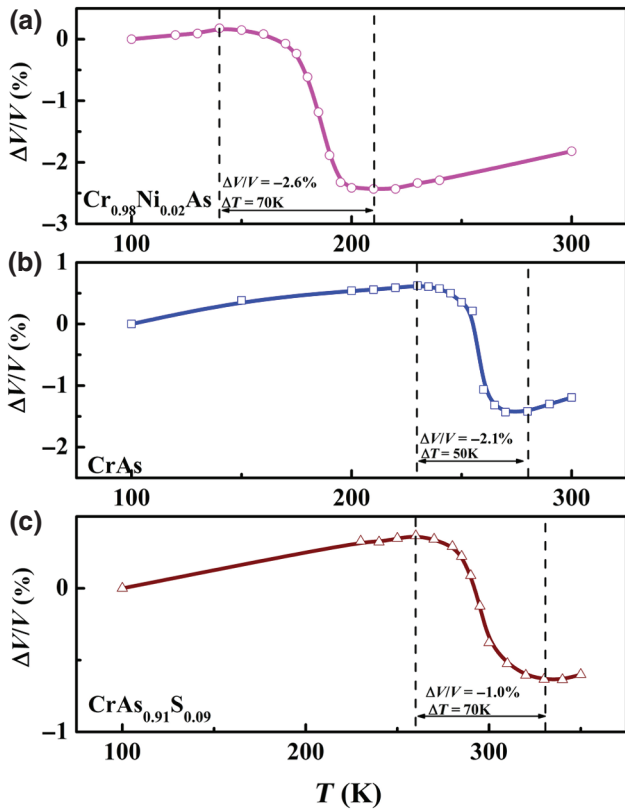


FIG. 2. Temperature dependence of volumetric thermal expansion $\Delta V/V$ (reference temperature: 100 K) for (a) $\text{Cr}_{0.98}\text{Ni}_{0.02}\text{As}$, (b) CrAs , and (c) $\text{CrAs}_{0.91}\text{S}_{0.09}$ determined by structural parameters. (Refined from XRD measurement results.)

maximum absolute values of $\Delta V/V$ are 2.6%, 2.1%, and 1.0% for $\text{Cr}_{0.98}\text{Ni}_{0.02}\text{As}$, CrAs , and $\text{CrAs}_{0.91}\text{S}_{0.09}$, respectively. It is noted that the absolute values of $\Delta V/V$ calculated from the cell parameters are all larger than the absolute values of $3\Delta L/L$ measured by dilatometer, which would be ascribed to the pores and other microstructural defects in the as-prepared samples [7].

Since NTE behavior occurs just around the magnetic phase transition temperature, it is necessary to perform neutron powder diffraction measurements to investigate the temperature evolution of the magnetic structures in CrAs -based compounds. Taking CrAs as an example, Figs. 3(a)–3(c) present the typical diffraction patterns at 200, 240, and 300 K, respectively. The Supplemental Material [27] presents the disappearance of magnetic peaks and shift of nuclear peaks during phase transition for $\text{Cr}_{0.98}\text{Ni}_{0.02}\text{As}$, CrAs , and $\text{CrAs}_{0.91}\text{S}_{0.09}$, respectively. The magnetic moments of Cr atoms and lattice parameters of CrAs -based compounds at these different temperatures are calculated by using the Rietveld refinement method and are shown in Fig. 4. Results of refinement fitting at 180 K ($\text{Cr}_{0.98}\text{Ni}_{0.02}\text{As}$), 200 K (CrAs), and 280 K ($\text{CrAs}_{0.91}\text{S}_{0.09}$) show that Cr atoms are magnetically ordered in the noncollinear double

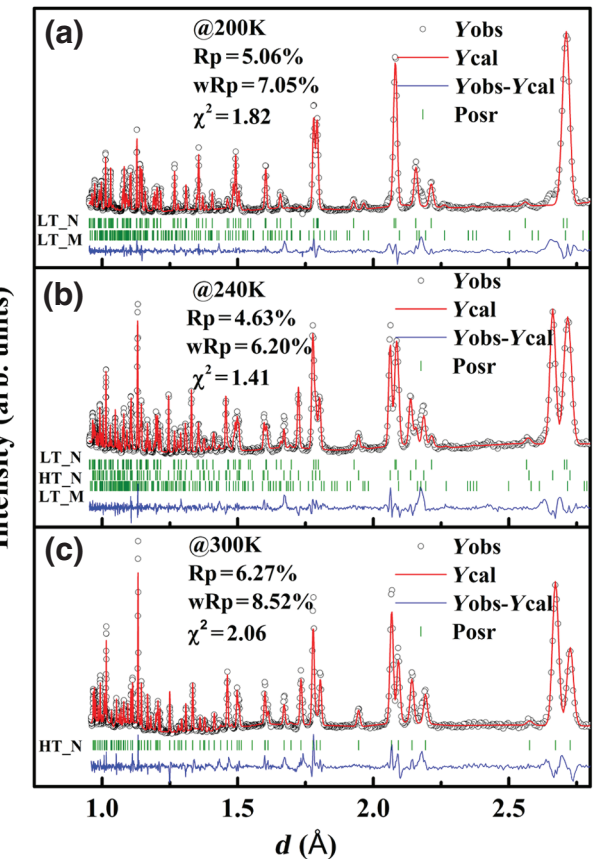


FIG. 3. Nuclear and magnetic peak fits at (a) 200 K, (b) 240 K, and (c) 300 K. The circles show the experimental intensities (Y_{obs}), the upper solid line shows the calculated intensities (Y_{calc}), and the lower solid line is the difference between the observed and calculated intensities ($Y_{\text{obs}} - Y_{\text{calc}}$). The vertical bars mark the angular positions of the nuclear Bragg peaks of phase_LT (LT_N), magnetic Bragg peaks of phase_LT (LT_N), and nuclear Bragg peaks of phase_HT (HT_N). R_p is the reliable factor of profile, wR_p is the weighted R factor of profile.

helimagnetic structure with the Cr magnetic moments of $1.29(4)\ \mu_B$ ($\text{Cr}_{0.98}\text{Ni}_{0.02}\text{As}$), $1.45(4)\ \mu_B$ (CrAs), and $1.50(5)\ \mu_B$ ($\text{CrAs}_{0.91}\text{S}_{0.09}$) lying in the a - b plane, which is in accordance with previous work [17,28]. As the temperature increases to the phase transition region, two crystal phases with the same crystal structure but different lattice constants coexist. When the temperature arrives at 300 K, only one crystal phase is observed. For the coexisting two crystal phases, the one for which the changing rule is valid at 180 K ($\text{Cr}_{0.98}\text{Ni}_{0.02}\text{As}$), 200 K (CrAs), 280 K ($\text{CrAs}_{0.91}\text{S}_{0.09}$) is marked as the low temperature phase (phase_LT) while the one that is valid at 300 K is marked as the high temperature phase (phase_HT). As temperature increases from the low temperature to 300 K, the fraction of phase_HT changes monotonously from zero to 100%. It should be noted that the magnetic order exists in phase_LT only, so the appearance of phase_HT means the breaking of magnetic order. As shown in Fig. 4, it is

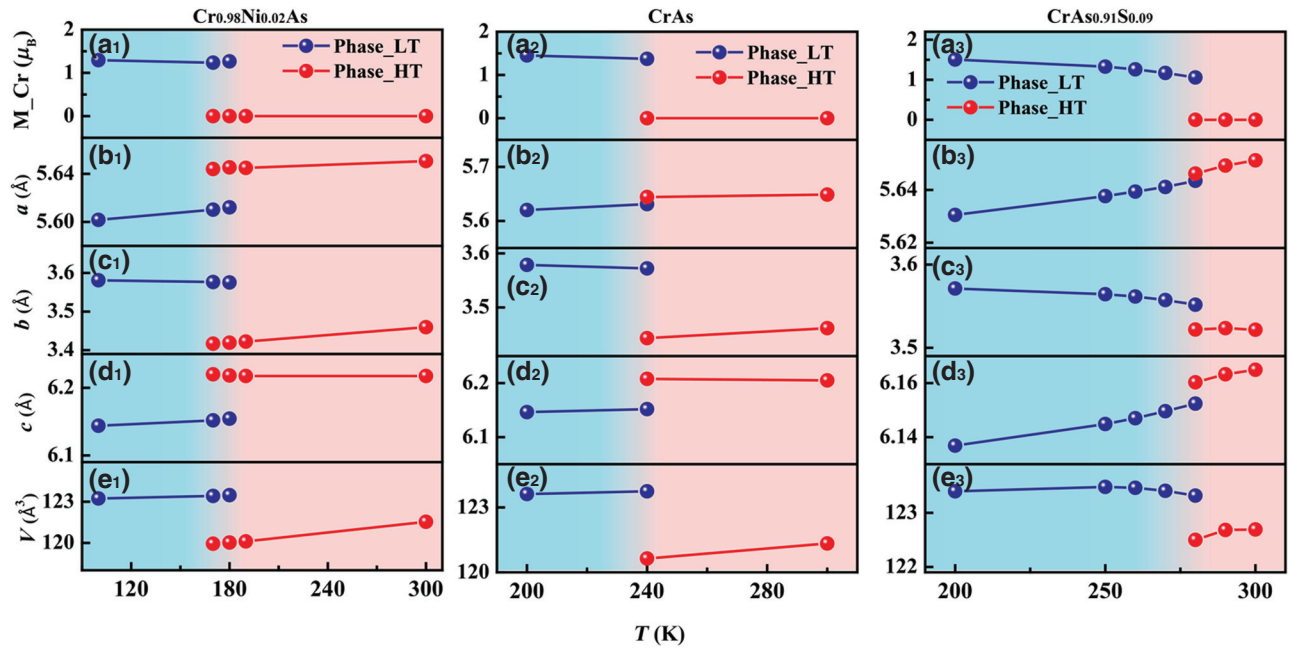


FIG. 4. (a₁-₃) Temperature dependence of Cr magnetic moment. (b₁-₃), (c₁-₃), (d₁-₃), (e₁-₃) Temperature dependence of lattice parameters a , b , c and the unit-cell volume V for Cr_{0.98}Ni_{0.02}As, CrAs, and CrAs_{0.91}S_{0.09}. (Refined from neutron powder diffraction data.)

obvious that the transition of the magnetic state is accompanied with the changes in lattice parameters and unit-cell volume. Different from the little jumps of the lattice parameter for the a axis and c axis, a sharp drop is observed in the b axis at 180, 240, and 280 K for Cr_{0.98}Ni_{0.02}As, CrAs, and CrAs_{0.91}S_{0.09}, respectively, further demonstrating that the NTE effect in CrAs is closely related to its AFM phase transition. The anomalous thermal expansion behaviors in CrAs originate from the strong correlations between magnetism and lattice vibrations. Due to the contribution of a phonon, a compound usually exhibits a positive thermal expansion behavior with increasing temperature. In CrAs-based compounds, the appearance of a magnetic moment below T_N is in favor of an increased volume, resulting in a magnetovolume effect. Since the NTE from magnetic contributions is larger than the positive thermal expansion from lattice phonon vibration, a NTE effect is observed during the phase transition region of CrAs-based compounds. Furthermore, we can deduce that the magnetovolume-effect-induced large decrease in the b axis is the origin of the giant NTE effect in CrAs-based compounds.

The abnormal antiferromagnetic transition in CrAs-based compounds is attributed to the variation of the occupied states of $3d$ electrons, which is also the origin of the sharp change in the b axis [28]. According to the theory proposed by Goodenough [30], the orbital states of Cr-based alloys are determined by a critical value ($R_c \sim 3.18$ Å) of the Cr-Cr distance, above or below which the $3d$ orbitals are in localized or collective states,

respectively. In the case of CrAs, the $3d$ orbitals are split into d_{z^2} , d_{xy} , $d_{x^2-y^2}$, d_{xz} , and d_{yz} orbitals ($x||b$ axis, $y||c$ axis, and $z||a$ axis), and the $d_{x^2-y^2}$ orbital is related to the change of the b axis [28]. At high temperatures (above T_N), the energy of the $d_{x^2-y^2}$ orbital (along the b axis and c axis) [28] rises above the Fermi surface, which prevents the occupation of electrons. However, if the temperature is below T_N , the electrons can occupy the $d_{x^2-y^2}$ orbital. On this occasion, the localized electrons occupying the $d_{x^2-y^2}$ orbital would result in an electrostatic repulsion along this direction, which is responsible for the sharp increase in the b axis in the LT phase [28]. It is worth pointing out that the localized electrons occupying the $d_{x^2-y^2}$ orbital have a negligible effect on the c axis because the Cr-Cr distance in this direction is far larger than that along the b axis [28].

As mentioned above, NTE material that has high thermal conductivity is more desirable in some practical applications [3,4]. In addition, NTE material with a high electrical conductivity is also a key component for the design of electronic devices with high system reliability [3,4]. Considering the aforementioned two requirements, the thermal and electrical conductivities for Cr_{0.98}Ni_{0.02}As, CrAs, and CrAs_{0.91}S_{0.09} samples are measured as a function of temperature. As shown in Fig. 5 and the Supplemental Material [27], the temperature-dependent electrical conductivity measurement indicates that this NTE material is of a metallic character and the electrical conductivity is at a level of about $1\text{--}3 \times 10^3$ (Ω cm)⁻¹, which can be seen from Fig. 5 and the Supplemental Material [27].

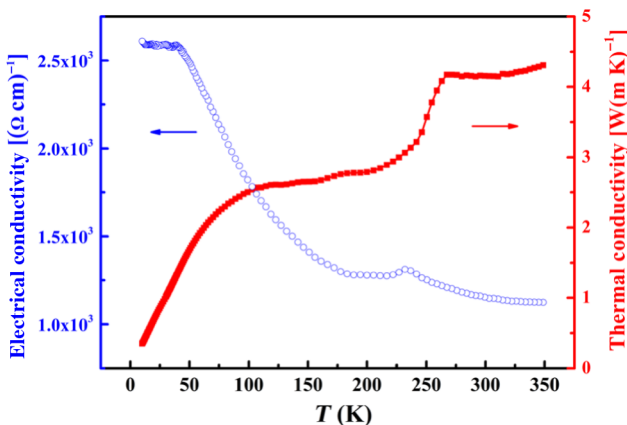


FIG. 5. Temperature dependence of thermal conductivity and electrical conductivity for CrAs.

The values of thermal conductivity are 5.1, 4.2, and 2.6 W (m K)^{-1} at room temperature for $\text{Cr}_{0.98}\text{Ni}_{0.02}\text{As}$, CrAs, and $\text{CrAs}_{0.91}\text{S}_{0.09}$, respectively. These values are much higher than that of a typical oxide NTE material, ZrW_2O_8 ($0.51 \text{ W (m K)}^{-1}$) [31] and comparable with that of $\text{Mn}_3\text{Ga}_{0.9}\text{Sn}_{0.1}\text{N}$ ($3.25 \text{ W (m K)}^{-1}$) [32]. It is worth noting that the thermal conductivity in CrAs-based compounds stems from the contributions of electrons and phonons. Taking CrAs as an example, as shown in Fig. 5, the anomalies for the thermal and electrical conductivities of the CrAs sample around T_N are quite different. In contrast with the sharp increase in the thermal conductivity, the electrical conductivity only shows a small peak around T_N . Thus, the sharp increase in thermal conductivity around T_N is mainly ascribed to the difference between the phonon contributions from the LT phase and the HT phase, since the electrical conductivity does not change a lot at this temperature. In addition, these anomalies further suggest the intrinsic interplay among structural, magnetic, and electronic properties in this system. In practical applications, NTE materials are likely to work in a magnetic condition, so the ferromagnetic materials possessing giant magnetostriction are unfavorable [4]. In this sense, the AFM CrAs-based compounds are advantageous since their dimensions are insensitive to the external magnetic field [4].

IV. CONCLUSION

In summary, NTE properties are systematically investigated in the AFM CrAs-based compounds. By optimizing the chemical composition, this system can show a giant NTE in a broad temperature region of 218 K, including room temperature. In the case of $\text{CrAs}_{0.91}\text{S}_{0.09}$, a large α of -28.3×10^{-6} together with a broad NTE operation-temperature window of 98 K are obtained around room temperature. In addition, the CrAs-based compounds exhibit large thermal and electrical conductivities and their

dimensions are insensitive to the magnetic field. All these excellent characteristics suggest their potential applications as NTE materials, particularly for compensating the materials used in the magnetic field environment.

ACKNOWLEDGMENTS

We acknowledge support by the Institute of Nuclear Physics and Chemistry in providing beam time on neutron powder diffraction measurements. This work was supported by National Key Research and Development Program of China (Grant No. 2017YFB0702701) and National Natural Science Foundation of China (Grants No. 51371095, No. 51501170, No. 51871019, No. 11674008, and No. 11574322).

Y. Hu, X.Q. Zheng, and G.D. Ma contributed equally to this work.

- [1] J. S. Evans, Z. Hu, J. Jorgensen, D. Argyriou, S. Short, and A. Sleight, Compressibility, phase transitions, and oxygen migration in zirconium tungstate, ZrW_2O_8 , *Science* **275**, 61 (1997).
- [2] Y. M. Hao, Y. Gao, B. Wang, J. P. Qu, Y. X. Li, J. F. Hu, and J. C. Deng, Negative thermal expansion and magnetic properties of $\text{Y}_2\text{Al}_3\text{Fe}_{14-x}\text{Mn}_x$ compounds, *Appl. Phys. Lett.* **78**, 3277 (2001).
- [3] R. J. Huang, Y. Y. Liu, W. Fan, J. Tan, F. R. Xiao, L. H. Qian, and L. F. Li, Giant negative thermal expansion in NaZn_{13} -type $\text{La}(\text{Fe}, \text{Si}, \text{Co})_{13}$ compounds, *J. Am. Chem. Soc.* **135**, 11469 (2013).
- [4] J. Chen, L. Hu, J. X. Deng, and X. R. Xing, Negative thermal expansion in functional materials: Controllable thermal expansion by chemical modifications, *Chem. Soc. Rev.* **44**, 3522 (2015).
- [5] X. G. Zheng, H. Kubozono, H. Yamada, K. Kato, Y. Ishiwata, and C. N. Xu, Giant negative thermal expansion in magnetic nanocrystals, *Nat. Nanotechnol.* **3**, 724 (2008).
- [6] J. Chen, K. Nittala, J. S. Forrester, J. L. Jones, J. X. Deng, R. B. Yu, and X. R. Xing, The role of spontaneous polarization in the negative thermal expansion of tetragonal PbTiO_3 -based compounds, *J. Am. Chem. Soc.* **133**, 11114 (2011).
- [7] M. Azuma, W. T. Chen, H. Seki, M. Czapski, S. Olga, K. Oka, M. Mizumaki, T. Watanuki, N. Ishimatsu, and N. Kawamura, Colossal negative thermal expansion in BiNiO_3 induced by intermetallic charge transfer, *Nat. Commun.* **2**, 347 (2011).
- [8] K. Takenaka, Y. Okamoto, T. Shinoda, N. Katayama, and Y. Sakai, Colossal negative thermal expansion in reduced layered ruthenate, *Nat. Commun.* **8**, 14102 (2017).
- [9] A. L. Goodwin, D. A. Keen, and M. G. Tucker, Large negative linear compressibility of $\text{Ag}_3[\text{Co}(\text{CN})_6]$, *Proc. Natl. Acad. Sci. USA* **105**, 18708 (2008).
- [10] Y. Y. Zhao, F. X. Hu, L. F. Bao, J. Wang, H. Wu, Q. Z. Huang, R. R. Wu, Y. Liu, F. R. Shen, and H. J. Kuang, Giant negative thermal expansion in bonded MnCoGe-based

- compounds with Ni₂In-type hexagonal structure, *J. Am. Chem. Soc.* **137**, 1746 (2015).
- [11] S. Fujieda, A. Fujita, K. Fukamichi, Y. Yamazaki, and Y. Iijima, Giant isotropic magnetostriction of itinerant-electron metamagnetic La(Fe_{0.88}Si_{0.12})₁₃H_y compounds, *Appl. Phys. Lett.* **79**, 653 (2001).
- [12] Q. B. Hu, Y. Hu, Y. Fang, D. H. Wang, Q. Q. Cao, Y. T. Yang, J. Li, and Y. W. Du, Large magnetostrain in magnetic-field-aligned Mn_{0.965}CoGe compound, *AIP Adv.* **7**, 056430 (2017).
- [13] Y. Sun, C. Wang, Y. C. Wen, L. H. Chu, M. Nie, and F. S. Liu, Negative thermal expansion and correlated magnetic and electrical properties of Si-doped Mn₃GaN compounds, *J. Am. Ceram. Soc.* **93**, 650 (2010).
- [14] K. Takenaka and H. Takagi, Giant negative thermal expansion in Ge-doped anti-perovskite manganese nitrides, *Appl. Phys. Lett.* **87**, 261902 (2005).
- [15] A. F. Andresen and J. Engebretsen, Magnetic structure and properties of CrAs, *Acta Chem. Scand.* **25**, 1703 (1971).
- [16] H. Watanabe, N. Kazama, Y. Yamaguchi, and M. J. Ohashi, Magnetic structure of CrAs and Mn-substituted CrAs, *J. Appl. Phys.* **40**, 1128 (1969).
- [17] Y. Shen, Q. S. Wang, Y. Q. Hao, B. Y. Pan, Y. Feng, Q. Z. Huang, L. W. Harriger, J. B. Leao, Y. Zhao, R. M. Chisnell, J. W. Lynn, H. B. Cao, J. P. Hu, and J. Zhao, Structural and magnetic phase diagram of CrAs and its relationship with pressure-induced superconductivity, *Phys. Rev. B* **93**, 060503(R) (2016).
- [18] W. Wu, J. Cheng, K. Matsubayashi, P. Kong, F. Lin, C. Jin, N. Wang, Y. Uwatoko, and J. Luo, Superconductivity in the vicinity of antiferromagnetic order in CrAs, *Nat. Commun.* **5**, 5508 (2014).
- [19] H. Kotegawa, S. Nakahara, H. Tou, and H. Sugawara, Superconductivity of 2.2 K under pressure in helimagnet CrAs, *J. Phys. Soc. Jpn.* **83**, 093702 (2014).
- [20] L. Keller, J. S. White, M. Frontzek, P. Babkevich, M. A. Susner, Z. C. Sims, A. S. Sefat, H. M. Rønnow, and C. Ruegg, Pressure dependence of the magnetic order in CrAs: A neutron diffraction investigation, *Phys. Rev. B* **91**, 020409 (2015).
- [21] T. Suzuki and H. Ido, 3D metal-substitution effects on magnetic and crystallographic properties of CrAs, *J. Appl. Phys.* **69**, 4624 (1991).
- [22] T. Suzuki and H. Ido, Spontaneous magnetostriction of CrAs_{1-x}S_x compounds, *J. Magn. Magn. Mater.* **140**, 149 (1995).
- [23] A. C. Larson and R. B. Von Dreele, *General Structure Analysis System (GSAS). Report LAUR 86-748* (Los Alamos National Laboratory, Los Alamos, NM, 2000).
- [24] G. Sun, C. Zhang, B. Chen, J. Gong, and S. Peng, A new operating neutron scattering facility CMRR in China, *Neutron News* **27**, 21 (2016).
- [25] K. Kanaya, S. Abe, H. Yoshida, K. Kamigaki, and T. Kaneko, Magnetic and structural properties of pseudo-binary compounds CrAs_{1-x}P_x, *J. Alloys Compd.* **383**, 189 (2004).
- [26] K. Motizuki, H. Ido, T. Itoh, and M. Morifushi, *Electronic Structure and Magnetism of 3D-Transition Metal Pnictides* (Springer, Berlin, Germany, 2009), p. 46.
- [27] See Supplemental Material at <http://link.aps.org/supplemental/10.1103/PhysRevApplied.12.034027> for magnetic susceptibility, DSC measurements, x-ray diffraction patterns, unit-cell volume, the lattice parameters, nuclear and magnetic peaks, magnetostriction, and electrical and thermal conductivity results.
- [28] H. Boller and A. Kallel, First order crystallographic and magnetic phase transition in CrAs, *Solid State Commun.* **9**, 1699 (1971).
- [29] K. Takenaka, K. Asano, M. Misawa, and H. Takagi, Negative thermal expansion in Ge-free antiperovskite manganese nitrides: Tin-doping effect, *Appl. Phys. Lett.* **92**, 011927 (2008).
- [30] J. B. Goodenough, Tech. Rept. No.234, Lincoln Laboratory MIT (1963).
- [31] C. A. Kennedy and M. A. White, Unusual thermal conductivity of the negative thermal expansion material, ZrW₂O₈, *Solid State Commun.* **134**, 271 (2005).
- [32] L. Q. Zhang, D. L. Wang, J. Tan, W. Li, W. Wang, R. J. Huang, and L. F. Li, Sn-doped Mn₃GaN negative thermal expansion material for space applications, *Rare Metal Mat. Eng.* **43**, 1304 (2014).